

Resorc[4]arene Modifiers for Supramolecular Site-Directed Immobilization of Antibodies on Multi-Walled Carbon Nanotubes

Francesca Polli,^[a] Gabriele Cianfoni,^[a, b] Rem Elnahas,^[c] Laura Mangiardi,^[a, b] Francesca A. Scaramuzzo,^[d] Silvia Cammarone,^[a] Deborah Quaglio,^{*[a]} Andrea Calcaterra,^{*[a]} Marco Pierini,^[a] Franco Mazzei,^[a] Robertino Zanoni,^[c] Bruno Botta,^[a] and Francesca Ghirga^[a]

One of the main problems in developing immunosensors featuring carbon nanotubes (CNTs) is immobilizing antibodies (Abs) onto the CNT surface to afford selective binding to target antigens (Ags). In this work, we developed a practical supramolecular Ab conjugation strategy based on resorc[4]arene modifiers. To improve the Ab orientation on the CNTs surface and optimizing the Ab/Ag interaction, we exploited the host-guest approach by synthesizing two newly resorc[4]arene linkers **R1** and **R2** via well-established procedures. The upper rim was decorated with eight methoxyl groups to promote selective recognition of the fragment crystallizable (F_c) region of the Ab. Moreover, the lower rim was functionalized with 3-bromopropoxy or 3-azidopropoxy sub-

stituents to bind the macrocycles on the multi-walled carbon nanotubes (MWCNTs) surface. Accordingly, several chemical modifications of MWCNTs were evaluated. After the morphological and electrochemical characterization of nanomaterials, the resorc[4]arene-modified MWCNTs were deposited onto a glassy carbon electrode surface to evaluate their potential applicability for label-free immunosensor development. The most promising system showed an improved electrode active area (A_{EL}) of almost 20% and a site-oriented immobilization of the SARS-CoV-2 spike protein S1 antibody (Ab-SPS1). The developed immunosensor revealed a good sensitivity ($23.64 \mu\text{A mL}^{-1} \text{cm}^{-2}$) towards the SPS1 antigen and a limit of detection (LOD) of 1.01 ng mL^{-1} .

Introduction

One of the best platforms for several new technologies is carbon nanotubes (CNTs), which aim to satisfy the increasingly demanding standards for clinical and diagnostic tests required for breakthroughs in medicine.^[1] A variety of sensors based on CNTs have been developed in recent years, such as gas


sensors,^[2] fiber-optic sensors,^[3] chemical sensors,^[4] and immunosensors.^[5] Although pristine CNTs exhibit high sensitivity to a wide variety of chemical signals, they lack selectivity.^[6,7] The ability to modify the surface of CNT-based technologies to impart selective binding to specific analytes is essential to their success.^[6,8] To improve selectivity of CNTs, surface modification by covalent or non-covalent functionalization with suitable molecules,^[9] such as polymers,^[10,11] metal nanoparticles,^[12–14] and biomolecules,^[15–17] has been exploited. Although non-covalent functionalization methods can generate selectivity without affecting the chemical properties of CNTs, they generally do not result in sufficiently robust materials for harsh environment applications. Supramolecular chemistry is a powerful surface modification tool to achieve high selectivity and sensitivity in sensor systems.^[18,19] The large pool of macrocycles available, with their synthetic modularity and different complexation properties, has represented an effective sensor design strategy.^[18,20] Among them, resorcinol-derived cyclic oligomers belonging to the calixarene family, namely resorcarenes, have attracted considerable attention as versatile macromolecular receptors with unique structure and complexation properties.^[21–24] The recognition features of such macrocycles towards a specific class of analytes can be addressed by inserting selective functional groups on both the upper and lower rims.^[19,25–27] In the last two decades, several studies have been focused on the use of calixarene-type macrocycles in the development of immunosensors to maximize the amount of the active immobilized antibodies (Abs) in the proper “end-on” orientation, thus promoting the


[a] F. Polli, G. Cianfoni, Dr. L. Mangiardi, S. Cammarone, Dr. D. Quaglio, Dr. A. Calcaterra, Prof. M. Pierini, Prof. F. Mazzei, Prof. B. Botta, Dr. F. Ghirga
 Department of Chemistry and Technology of Drugs
 Department of Excellence 2018–2022
 Sapienza-University of Rome, P.le Aldo Moro 5, 00185 Rome (Italy)
 E-mail: deborah.quaglio@uniroma1.it
andrea.calcaterra@uniroma1.it

[b] G. Cianfoni, Dr. L. Mangiardi
 Center for Life Nano- and Neuro-Science@Sapienza
 Italian Institute of Technology
 Viale Regina Elena 291, 00161 Rome (Italy)

[c] R. Elnahas, Prof. R. Zanoni
 Department of Chemistry
 Sapienza-University of Rome
 P.le Aldo Moro 5, 00185 Rome (Italy)

[d] Dr. F. A. Scaramuzzo
 Department of Basic and Applied Sciences for Engineering
 Sapienza - University of Rome
 Via del Castro Laurenziano 7, 00161 Rome (Italy)

 Supporting information for this article is available on the WWW under <https://doi.org/10.1002/cbic.202300030>

 © 2023 The Authors. ChemBioChem published by Wiley-VCH GmbH. This is an open access article under the terms of the Creative Commons Attribution Non-Commercial NoDerivs License, which permits use and distribution in any medium, provided the original work is properly cited, the use is non-commercial and no modifications or adaptations are made.

accessibility of the fragment antigen-binding (F_{ab}) regions towards the antigen (Ag) detection (Figure 1A).^[19,28,29] Indeed, the host-guest (receptor) approach has proved a practical antibody immobilization procedure (Figure 1A). The introduction of artificial linkers on the sidewall of CNTs could lead to the selective recognition of the fragment crystallizable (F_c) region of the antibody by directing the antigen-binding F_{ab} fragment away from the CNTs surface. Notably, whereas several functionalized calixarenes have been employed as surface modifiers to favor the optimal antibody orientation, just a few resorcarenes have been developed for this purpose.^[19] In this work, to the best of our knowledge, we present for the first time cavitand-functionalized CNTs with improved Ab/Ag affinity. To this end, two newly resorc[4]arene architectures (R1 and R2, Figure 1B) were designed and synthesized to covalently functionalize the CNTs surface. By modifying the CNT sidewalls with the artificial linkers, we built chemiresistors having multi-walled carbon nanotubes (MWCNTs) as the conductive element. For this purpose, oxidized MWCNTs were chemically modified by inserting amino and propargyl functionalities. A less invasive approach was also investigated by directly functionalizing the pristine-MWCNTs *via* thermal 1,3-dipolar cycloaddition reaction followed by nitrogen extrusion. Eventually, the anchoring of the macrocycles to MWCNTs was achieved (namely, R1-MWCNTs, R2-MWCNTs, and R2-p-MWCNTs), and all the modified nano-

materials were fully characterized. The application of resorc[4]arene-MWCNTs for label-free electrochemical immunosensor development was investigated by modifying glassy carbon (GC) electrodes with nanomaterials. Finally, the molecular recognition properties of the most promising system, GC/R1-MWCNTs, were explored towards the absorption of the immunoglobulin G (IgG) antibodies specific for the SARS-CoV-2 spike protein S1 (Ab-SPS1). In this work, we demonstrated how the supramolecular antibody conjugation technique based on resorc[4]arene modifiers holds great promise for advancing diagnostic testing.

Results and Discussion

Design and synthesis of resorc[4]arene macrocycles R1 and R2.

Orientation and loading density of the immobilized antibodies govern F_{ab} accessibility and are critical to the analytical performance of several detection strategies.^[28,29] In our previous work, we demonstrated that surface modification by properly functionalized resorcarene macrocycles allows the optimal Ab orientation favoring the “end-on” configuration.^[23,28] To construct a CNT-based platform with improved selectivity, we rationally designed and synthesized two new resorc[4]arene architectures (R1 and R2, Figure 1B and Scheme 1). The upper rim of these bowl-shaped macro-

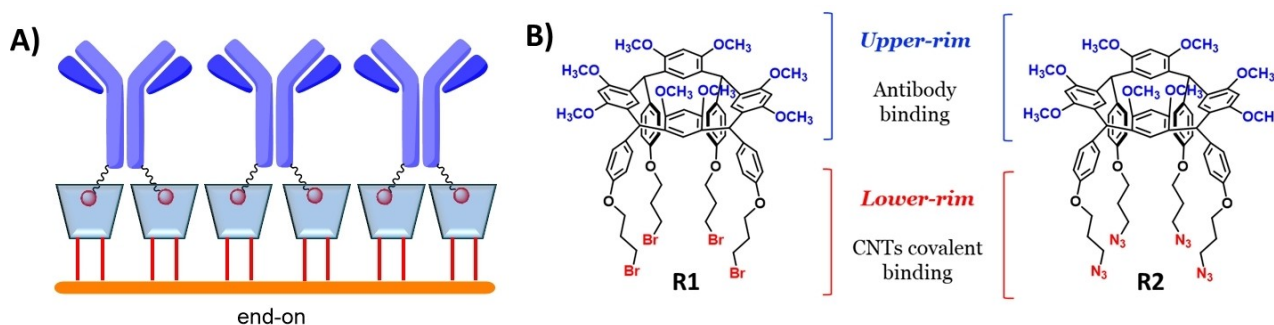
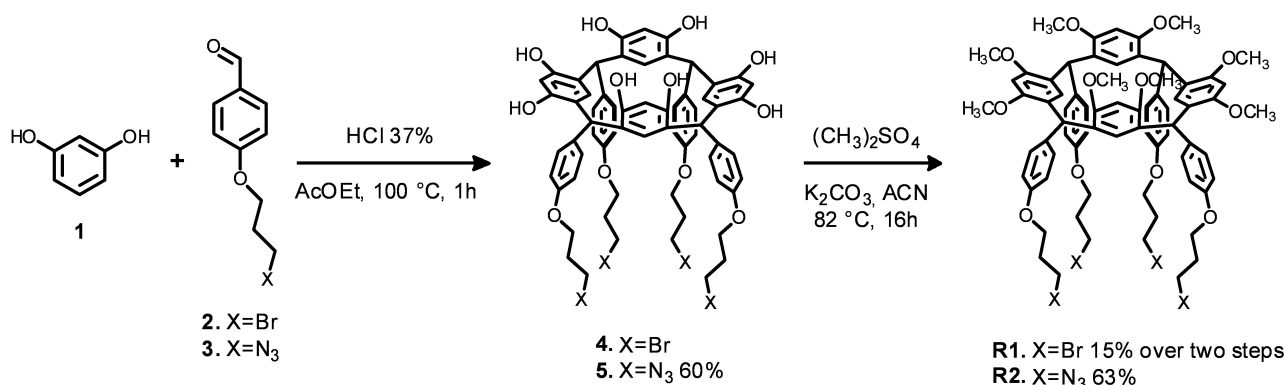


Figure 1. A) Host-guest (receptor) approach for the site-oriented antibody immobilization; B) Chemical structures of resorcarene-based supramolecular linkers R1 and R2.

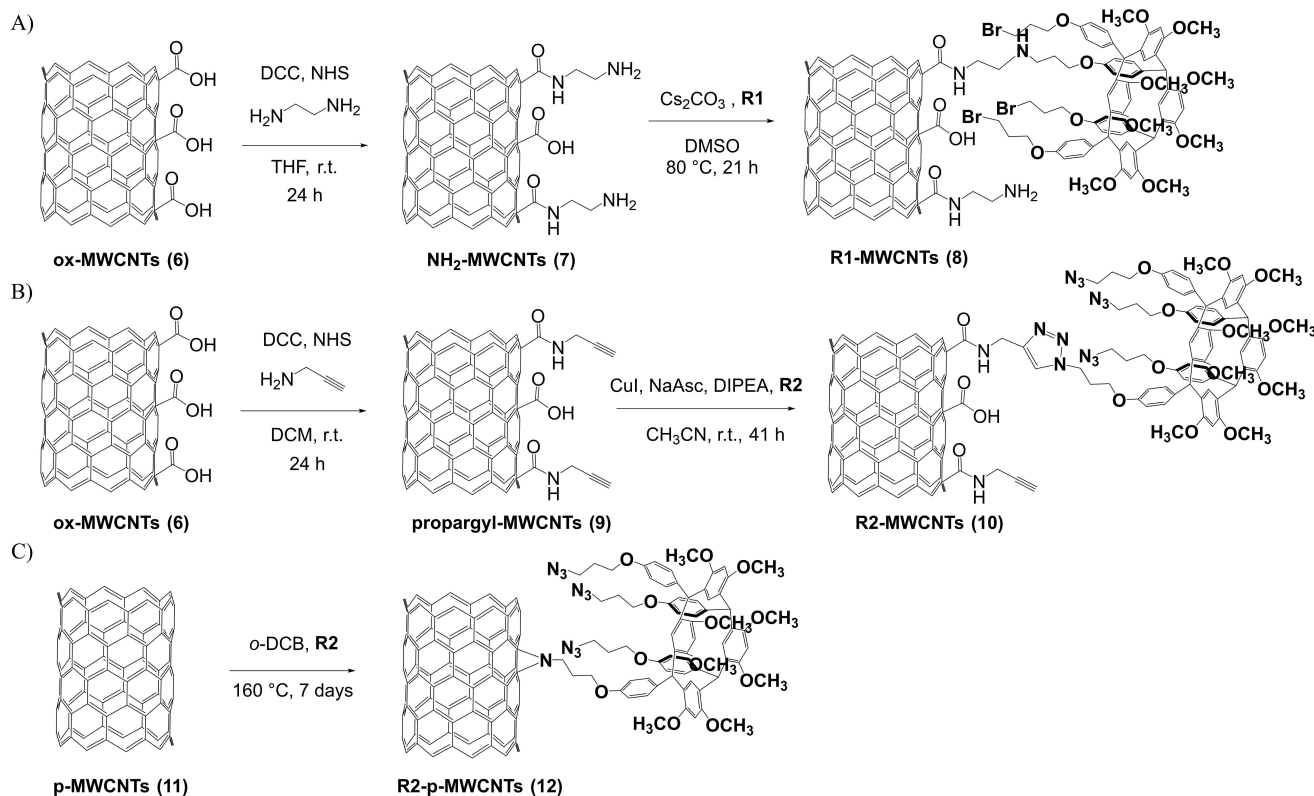


Scheme 1. Synthesis of resorcarene-based linkers R1 and R2.

cycles is decorated with eight methoxyl groups to tailor their recognition properties towards the F_c portion of Abs; the lower rim is featured by different functional moieties (i.e., 3-bromopropoxy or 3-azidopropoxy substituents) to covalently install the artificial linkers on the CNTs. The synthetic strategy employed to prepare **R1** and **R2** was based on the well-established acid catalyzed condensation reaction. Resorcinol (**1**) was allowed to react with benzaldehydes (**2**)^[30] and (**3**)^[31] by using concentrated hydrochloric acid (37%) to obtain the corresponding tail-derivatized resorcarenes (**4**) and (**5**) (Scheme 1). Free hydroxyl groups on the upper rim of **4** and **5** were further methylated by using dimethyl sulfate in the presence of potassium carbonate as the base.^[32] Since resorcarenene **4** showed poor solubility in a wide range of organic solvents, the methylation reaction was directly performed on the crude reaction mixture, achieving **R1** in 15% yield over two steps. The artificial linker **R2** was obtained with an overall yield of 38%. The structures of resorc[4]arenes **R1** and **R2** were confirmed by ^1H and ^{13}C Nuclear Magnetic Resonance (NMR) spectroscopies and by electrospray ionization high-resolution mass spectrometry (ESI-HRMS) (Supporting Information). The choice of ethyl acetate (AcOEt) as the tetramerization solvent was crucial to get the desired boat-like or "pinched cone" conformation featuring aryls in axial positions.^[33] In the ^1H and ^{13}C NMR spectra of **R1** and **R2**, the distribution pattern includes two signals for both the aromatic CH_e (external) and CH_i (internal) of the resorc[4]arene cavity,

whereas the methine groups give only one singlet. All these features are typically in agreement with C_{2v} symmetry.

Synthesis of the resorc[4]arene-MWCNTs. To develop highly sensitive and selective nanomaterials, we functionalized the surface of MWCNTs with linkers **R1** and **R2** by three different methodologies. The first two approaches consist in the derivatization of oxidized MWCNTs (ox-MWCNTs) with reactive functional groups such as amino or propargyl ending moieties. In particular, after the *in situ* activation of the carboxylic acid moieties by DCC/NHS system, the ox-MWCNTs (**6**) were allowed to react with ethylene diamine or propargylamine at room temperature to afford the sidewall amidated multi-walled carbon nanotubes namely NH_2 -MWCNTs (**7**) and propargyl-MWCNTs (**9**), respectively (Scheme 2A and 2B).^[34] These activation steps were followed by the covalent grafting of resorc[4]arene **R1** or **R2** on MWCNTs surface.^[35] **R1** was specifically anchored by the nucleophilic substitution reaction between the amino groups of the modified **7** and the alkyl bromide chains of the macrocycle (see Scheme 2A), to obtain the corresponding **R1-MWCNTs** (**8**).^[36] The modified nanomaterials were characterized by X-ray photoelectron spectroscopy (XPS) (Figure 2A). Upon such reaction, no significant change is expected either in the shape of N 1s peak or in its binding energy (BE), falling in the restricted range $399.5 \pm 0.4 \text{ eV}$,^[37] because of the close chemical similarity of N-H and N- CH_3 groups. This is confirmed by comparing the spectra in Figure 2A. XPS data on **R1** gave the expected atomic C/O ratio (theor: 72/12, exptl.: 6.0), while the O/Br relative intensity of



Scheme 2. Synthetic approach to modify MWCNTs with the supramolecular linkers **R1** and **R2**.

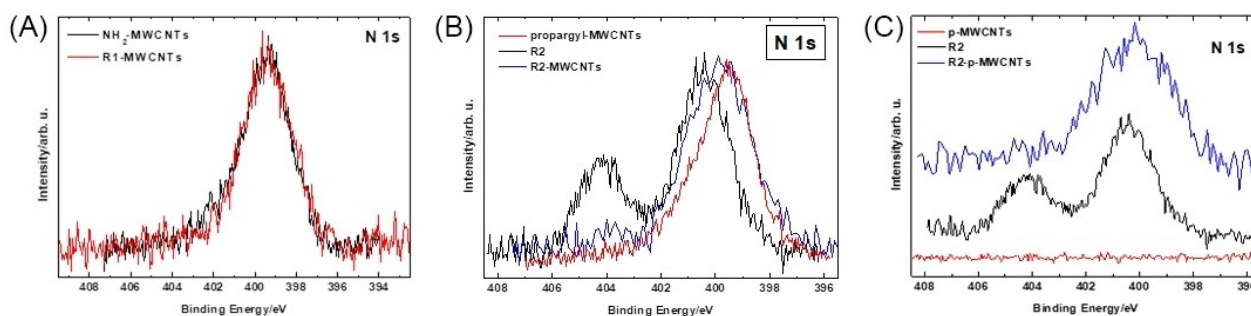


Figure 2. (A) Compared N 1s XPS peaks from **7** (black line) and **8** (red line); (B) a comparison between N 1s XPS peaks from **R2** (black line), **9** (red line), and **10** obtained via click-chemistry (blue line); in this last species, a residual presence of azido N^+ characteristic peak is evident at ~ 404 eV; (C) a comparison between N 1s XPS peaks from **R2** (black line), **11** (red line), and **12** obtained through thermolytic *in situ* generation of reactive nitrene from azido groups at 160°C (blue line).

bromine was about 50% lower than the expected value of 6 due to a partial loss of bromine under X-rays in high vacuum. A major clue to the successful anchoring of **R1** is the large variation in the O/N XPS ratio, which raised from 1.8 in **7** to 4.3 for **8**. A detailed analysis of XPS data revealed the extent of MWCNTs functionalization in two **R1** molecules anchored every 100 carbon atoms (Supporting Information).

Azidoresorcurene **R2** was grafted on **9** by copper catalyzed Huisgen 1,3-dipolar cycloaddition in the presence of sodium ascorbate, a known powerful linking reaction, affording the formation of **10** featuring a 1,2,3-triazole moiety, as confirmed by XPS analyses (Scheme 2B).^[38–40] A comparison among the photoemission regions for N 1s of the species involved in the functionalization step is reported in Figure 2B. The **R2** grafting on MWCNTs *via* click-chemistry reaction lead to a modification of the N 1s region of the XPS spectra of the four azido groups on the resorcurene lower rim. For each **R2** molecule anchored, one amido and one triazole groups are present, but only the latter results from the reaction. This means that the highest intensity in the N 1s peak must be represented by amido groups, as experimentally found. A tentative theoretical reconstruction of the N 1s peak by curve-fitting is shown and commented in Figure S5. The N 1s peak for **10** results from the simultaneous presence, in different percentages, of amido, azido and triazole functions. A triazole pentatomic ring contains two non-equivalent nitrogen atoms, expected at 400.7 and 401.7 eV, respectively, in a 2:1 ratio.^[41,42] In the N 1s spectrum for **10** (Figure 2B), the double peak of both **R2** and **9** are replaced by a complex peak with residual traces of the characteristic azido N^+ peak. The energy position and the general lineshape of this N 1s peak are consistent with the related literature findings for forming triazole rings on different surfaces.^[43,44] The successful functionalization is also supported by the drop in the quantitative C/O atomic ratio from 8.7 in the **9** to 4.2 in **10**, consistent with the introduction of **R2**, for which the C/O ratio is equal to 6. The extent of MWCNTs functionalization with **R2** was estimated 1–2 resorcurene units every 100 carbon atoms (Supporting Information).

The third functionalization approach involved the direct grafting of resorc[4]arene **R2** on pristine MWCNTs (**11**) through thermolytic *in situ* generation of reactive nitrene from azido groups using *o*-dichlorobenzene (*o*-DCB) as solvent at 160°C , to afford the corresponding **R2-p-MWCNTs** (**12**) (Scheme 2C).^[45]

The **R2** grafting on **11** was examined by XPS. The analysis was performed by comparing the N 1s photoemission regions for the species involved in the reaction (Figure 2C). In **12**, the N 1s lineshape is relatively wide, suggesting the co-presence of distinct species. No residual peak due to the azido N^+ component is traceable, suggesting that either the azido groups were all involved in the reaction, or the operating conditions were more drastic concerning the click-chemistry route, possibly favoring the decomposition of unreacted azido groups. This N 1s complex peak can be curve-fitted with two components, as shown in Figure S9, consistently with previous evidence on the formation of aziridine rings in MWCNTs.^[46] In the same report, a main N 1s peak assigned to aziridine units is accompanied by a shoulder at 1.7 eV higher binding energy, which was proposed to be due to amine carbonation in air.^[47] In the present case, the same energy separation was found where the binding energies for both components are rigidly shifted of 0.7 eV towards higher binding energies. This can account for the molecular bond of **R2** to MWCNTs, while in the mentioned report, aziridine rings are formed directly on MWCNTs. The same procedure outlined above for quantitative estimation of the extent of MWCNTs functionalization gives ~ 1 resorcurene unit anchored every 100 carbon atoms (see Supporting Information).

All the modified nanomaterials were also morphologically characterized by field emission scanning electron microscopy (FE-SEM) and atomic force microscopy (AFM) (Supporting Information).

Application of resorc[4]arene-MWCNTs for immunosensor development. To develop label-free and robust immunosensor devices, MWCNTs modified with the supramolecular linkers **R1** and **R2** were deposited on the Glassy Carbon Electrode (GCE) surface at three different concentrations (i.e., 1 mg mL^{-1} , 0.1 mg mL^{-1} , and 0.01 mg mL^{-1}). The electrochemical charac-

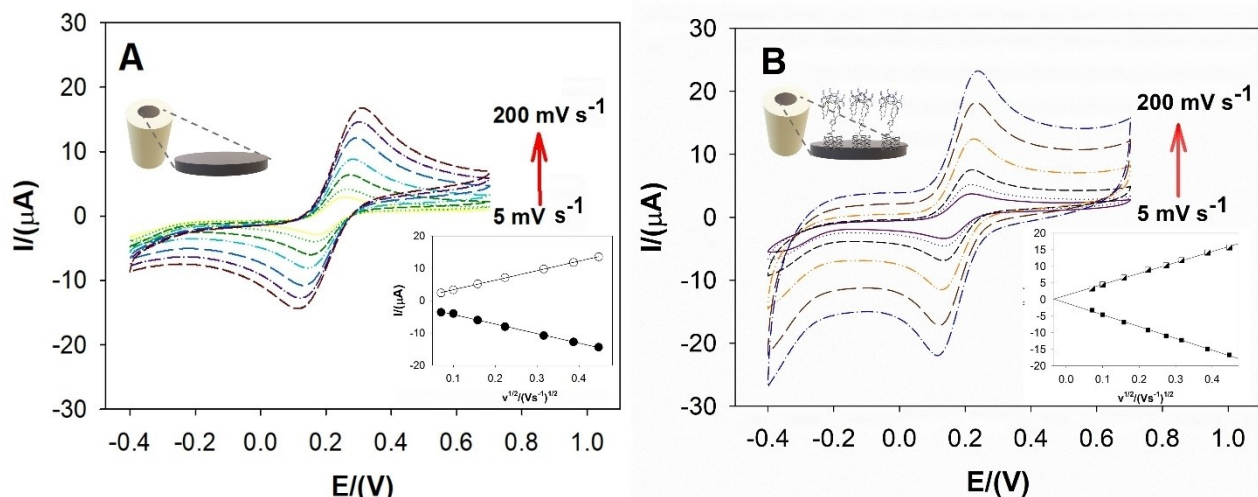


Figure 3. CV curves acquired in the 5–200 mV/s range and their fitted plots before (A) and after the modification (B) with GC/R1-MWCNTs.

terization was carried out by cyclic voltammetry (CV) and differential pulse voltammetry (DPV) measurements. On the basis of CV measurements (Figure 3), the best performance in terms of the current increase and reversibility of the system was obtained with GC/R1-MWCNTs compared with a bare GCE.^[48,49] Accordingly, DPV analysis revealed a signal increase of +62% in the anodic peak for the modified 8 glassy carbon electrodes and an improved electrode active area (A_{EL}) of almost 21% mm^2 , from 3.715 to 4.479 mm^2 (see Table 1).^[50,51]

	GC Bare	GC/R1-MWCNTs
A_{EL} [mm^2]	3.72 ± 0.07	4.48 ± 0.23
I [μA]	7.61 ± 0.30	12.32 ± 0.55
ΔE_{c-a} [mV]	90.18 ± 7.61	74.17 ± 3.45

The results obtained can be explained by the presence of resorcinarene molecules, leading to an increase in the capacitive contribution.^[52,53] On the contrary, no signal increase in DPV and CV measurements was observed for the 10 and 12, due to the weak adhesion and aggregation phenomena on the GCE surface. Notably, the best-performing system was further employed to develop a label-free electrochemical immunosensor for detecting spike protein S1 (SPS1).^[19,28,54]

To maximize the Ab-SPS1 (antibody for the SARS-CoV-2 spike protein S1) immobilization on GC/R1-MWCNTs, the optimal antibody concentration to be employed was assessed by DPV measurements. As shown in Figure 4A, the current intensity variation (ΔJ) was evaluated in the [Ab-SPS1] range of 0.1–1 $\mu\text{g mL}^{-1}$ and the antibody concentration of 0.2 $\mu\text{g mL}^{-1}$ was estimated as the best to optimize the Ab-SPS1 absorption with a good reproducibility. Inspection of the

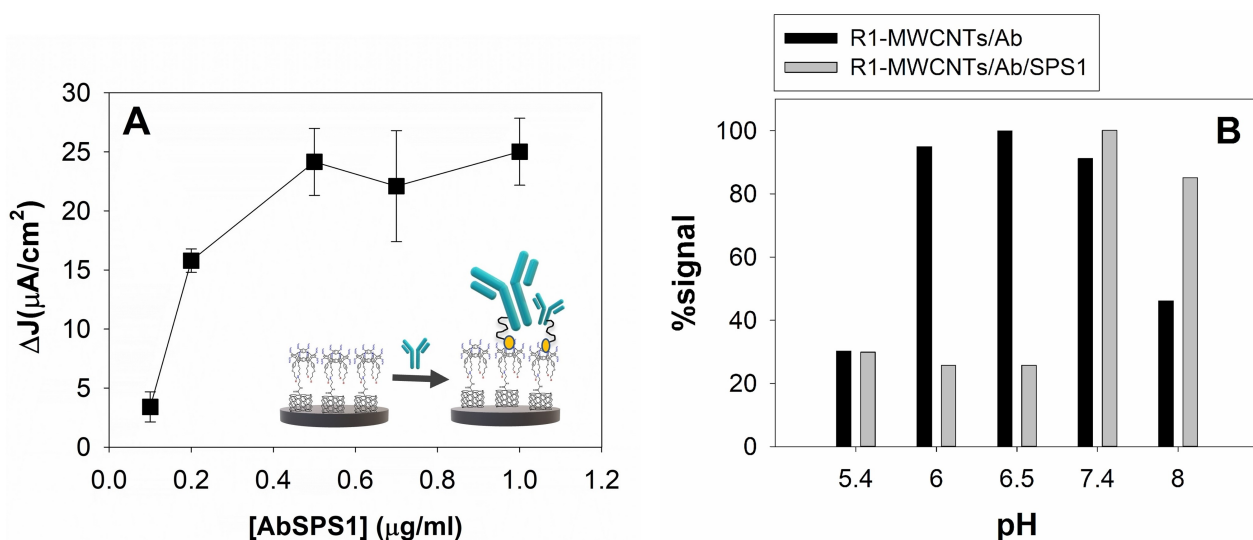


Figure 4. DPVs decrease after Ab-SPS1 absorption (A) in the concentration range 0.1–1 $\mu\text{g mL}^{-1}$ and (B) at pH 5.4–8.

relevant literature on calixarene-protein binding suggests the presence of different supramolecular interactions (i.e. electrostatic, cation- π , etc.).^[27,55,56] Among them dipole-dipole attractions play a crucial role in the site-oriented immobilization of Ab.^[28,55] Additionally, several studies demonstrated the ability of few neutral bowl-shaped receptors to form inclusion complexes with a variety of cationic molecules by creating cation- π interactions:^[57,58] this evidence can effectively sustain the supramolecular binding of the protonated side chains of basic amino acids decorating the F_c region of Ab to the electron-rich aromatic surface of resorc[4]arene linkers.^[56,59,60] To evaluate the potential ability of resorc[4]arene modifier to promote the "end-on" orientation of Ab guest *via* supramolecular interactions, the relevant dipole moments (DMs) of R1 and its derivative featuring an aminoethylacetamide moiety, mimicking the macrocycle anchorage to MWCNTs (structure 8 of Scheme 2), were estimated by theoretical calculation (for details see Supplementary Information). The corresponding values of 9.2 and 10.9 debye, DMs from the positive pole of the upper-rim to the negative one of the lower-rim, were obtained for R1 and R1-modified linkers, respectively. By comparing such DMs with those established for previously developed resorc[4]arenes able to favour site-directed immobilization of insulin antibody, ranging from 9.9 to 12.4 debye,^[26] the polarity of R1 and R1-modified macrocycles perfectly match with the ability to act as supramolecular receptors for the Ab-SPS1 guest. Moreover, with the purpose to evaluate the possible effect of pH on the Ab-SPS1 immobilization on GC/R1-MWCNTs, the % signal (as intensity current) was monitored as a function of increasing pH values. As reported in Figure 4B, the experimental data revealed a

correlation between Ab-SPS1 absorption and pH, improving the % signal in a pH range between 6–7.5. The obtained data suggest that the host-guest interaction between the F_c region of Ab and the upper rim of R1 is influenced by the protonation state of the basic amino acid sidechains at pH values below 7.5. A simple explanation is that Coulombic interactions are reduced at $\text{pH} > 7.5$, resulting in a rapid decrease in the % signal and, thus, in a lower affinity of F_c -Ab for the resorc[4]arene macromolecules (Figure 4B).^[28,54,61]

Considering the antigen binding, the maximum interaction was seen between pH 7.4 and 8. In contrast, at pH 5.4 the lowest antigen interaction occurred, as expected by observing the Ab immobilization level. Moreover, although a high Ab density was assessed, the modest percentage of signal loss caused by SPS1-AbSPS1 binding at pH 6–7.4 can be explained by considering the positive net charge provided by the SPS1 isoelectric point value at pH 7.4,^[62,63] which facilitates ferri/ferrocyanide diffusion.

In Table 2 are reported the intensity currents arising from the DPV experiments performed by adding SPS1 on unmodified- and R1-modified-MWCNTs electrodes. The results obtained evidence the almost constant value of current recorded in the presence of Ab/SPS1 with the unmodified-MWCNTs electrode.

To evaluate the resorc[4]arene-based immunosensor sensitivity towards antigen detection, analytical parameters such as limit of detection (LOD) and linear working range were determined. The DPV measurements were recorded in the presence of a redox pair ferri/ferrocyanide by applying different concentrations of SPS1 protein in the range of 0.1–100 ng mL^{-1} to the immunosensor surface, conveniently deactivated by using Bovine Serum Albumin (BSA).^[64] Figure 5 shows the recorded DPV profile (A) and the corresponding calibration curve and linear fit analysis (B), revealing a correlation coefficient of 0.973 in a linearity range from 3 to 100 ng mL^{-1} of SPS1.^[62,65] The developed system shows a sensitivity of 23.64 $\mu\text{A mL ng}^{-1} \text{cm}^{-2}$ and a LOD of 1.01 ng mL^{-1} .

Modification	GC/MWCNTs	GC/R1-MWCNTs
Bare	14.77	12.67
Ab/BSA	14.49	11.53
Ab/BSA/SPS1	14.26	9.76

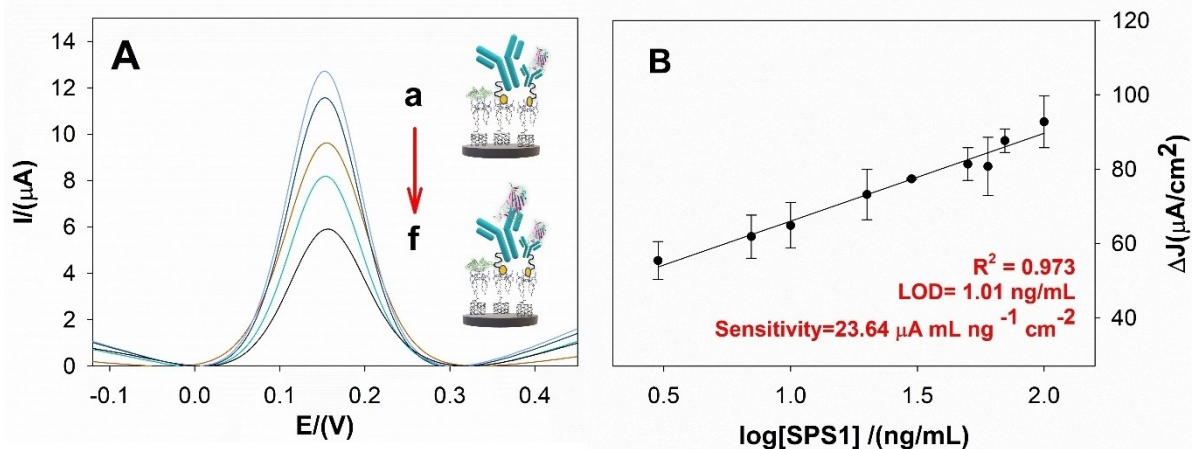


Figure 5. (A) DPV signal obtained after absorption of increasing concentration of SPS1 protein; (B) calibration curve obtained with standard SPS1 solutions.

The overall analytical features of the developed immunosensor demonstrate its potential broad application field.^[49,66,67]

Performance comparison between R1-MWCNTs- and ox-MWCNTs-based immunosensors toward site-directed immobilization

Comparing the results obtained with the R1-MWCNTs- and the ox-MWCNTs-based immunosensors, the former is much more sensitive than the latter, since no significant signal is observed until 10 ng/mL of SPS1 for the ox-MWCNTs platform. In the GC/R1-MWCNTs modified electrodes, a three times lower signal can be detected, confirming that the site-directed immobilization improves immunosensors performance (Figure 6).

Conclusions

In this work, we first developed a practical immobilization technique based on resorc[4]arene-modified MWCNTs. To improve the antibody orientation on the CNTs surface and optimize the Ab / Antigen (Ag) interaction, we exploited the host-guest (receptor) approach by synthesizing two newly resorc[4]arene linkers **R1** and **R2** via well-established procedures. The macrocycles were decorated on the upper rim with eight methoxyl groups to tailor their recognition properties towards the F_c portion of Abs and on the lower rim with different functional moieties (i.e., 3-bromopropoxy or 3-azidopropoxy substituents), to covalently install the artificial linkers on the CNTs. Three different methodologies were employed to chemically modify the surface of nanomaterials and the functionalization of amidated multi-walled carbon nanotubes, **7** and **9**, with resorc[4]arenes via nucleophilic substitution or copper-catalyzed azide/alkyne cycloaddition emerged as the most promising approach. XPS analyses

confirmed the covalent binding of the linkers **R1** and **R2** on the MWCNTs, by evaluating the N/O and C/O atomic ratios and comparing the N 1s peaks of the modified materials and precursors. The application of resorc[4]arene-MWCNTs for the development of label-free electrochemical immunosensors was investigated by modifying the GC electrodes with the nanomaterials. The most promising system GC/R1-MWCNTs showed an improved A_{EL} of almost 20.56% mm² and a site-oriented immobilization of Ab-SPS1, driven by both dipole-dipole and cation- π bonding interactions between the electron-rich aromatic surface of **R1** and the protonated side chains of basic amino acids located in the F_c-Ab portion. The developed immunosensor revealed a good sensitivity (23.64 μ A mL ng⁻¹ cm⁻²) towards the SPS1 antigen and a LOD of 1.01 ng mL⁻¹. Despite the most common covalent coupling approaches to immobilize antibodies on CNTs, our results demonstrated that the supramolecular antibody conjugation strategy based on resorc[4]arene-modifiers allow to obtain high Ab density optimizing the overall analytical properties of the developed immunosensors.

Experimental Section

General information. All solvents, reagents and nanomaterials for the synthesis of resorc[4]arenes and resorc[4]arene-MWCNTs were purchased from Merck KGaA (Darmstadt, Germany) or Carlo Erba Reagenti, (Milano, Italy) and used without further purification unless otherwise stated. For the electrochemical measurements, sodium phosphate monobasic (NaH₂PO₄), sodium phosphate dibasic (Na₂HPO₄), potassium chloride (KCl), potassium ferricyanide trihydrate (K₃Fe[CN]₆·3H₂O), potassium ferrocyanide hexahydrate (K₄Fe[CN]₆·6H₂O), 2-(*N*-morpholino)ethanesulfonic acid (MES), 4-(2-hydroxyethyl)-1-piperazineethanesulfonic acid (HEPES) were obtained from Sigma Aldrich (St. Louis, MO, USA). SARS-CoV-2 (2019-nCoV) Spike S1-His Recombinant Protein and SARS-CoV-2 (2019-nCoV) Spike S1 Antibody Rabbit Monoclonal Antibody (Ab-SPS1) were purchased from Sino Biological (Beijing, China). GC electrodes were obtained from Metrohm (Switzerland). All reactions for the synthesis of macrocycles were monitored by thin-layer chromatography (TLC), and silica gel plates with fluorescence F254 were used. ¹H NMR and ¹³C NMR spectra were recorded using a Bruker 400 Ultra Shield™ spectrometer (operating at 400 MHz for ¹H and 101 MHz for ¹³C). Chemical shifts are reported in parts per million (ppm). Multiplicities are reported as follows: singlet (s), doublet (d), triplet (t), pentet (p), and multiplet (m). Melting points were measured in open capillaries on a Büchi Melting Point B-545 apparatus. High-resolution mass spectra (HR-MS) were acquired on a hybrid quadrupole-Orbitrap Q Exactive mass spectrometer, Thermo Fischer Scientific (Waltham, Massachusetts, US). The spectra were acquired with a resolution of 35000, an AGC target of 1e6, a maximum injection time of 50 s, a sample flow rate of 20 μ L/min, a sheath gas flow rate of 8 mL/min, a capillary temperature of 320 °C and a S-Lens RF level of 50. For positive ionization mode, the following parameters have been set as reported: spray voltage at 4.0 kV and sheath gas flow rate at 8 mL/min. Negative mode ionization was performed with a spray voltage of 3.2 kV and a sheath gas flow rate of 7 mL/min. The electrochemical measurements were collected using a mAUTOLAB PGSTAT204 (Metrohm, Herisau, Switzerland) controlled by NOVA 2.1 software on a Windows pc.

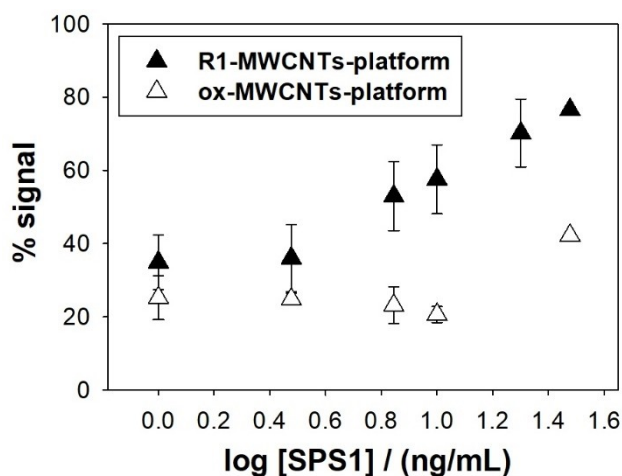


Figure 6. Comparison between % signal decays obtained after SPS1 interaction on the R1/MWCNTs-based platform and MWCNTs-COOH.

Synthesis of 4-(3-Bromopropoxy)benzaldehyde (2). Compound 2 was prepared according to the reported procedure.²⁹ The crude was purified by silica gel flash chromatography (petroleum ether 100%→petroleum ether/ethyl acetate 95:5) to afford compound 2 in 81% yield as a light yellow solid. The spectroscopical data were identical to those reported in literature.^[68]

4-(3-Bromopropoxy)benzaldehyde (2). R_f : 0.63, Petroleum ether/ethyl acetate 7:3. $^1\text{H NMR}$ (400 MHz, CDCl_3) δ 9.86 (s, 1 H), 7.84–7.79 (m, 2 H), 7.01–6.97 (m, 2 H), 4.18 (t, J = 5.8 Hz, 2 H), 3.59 (t, J = 6.4 Hz, 2 H), 2.37–2.29 (m, 2 H).

Synthesis of Resorc[4]arene 4. Concentrated HCl (37%, 3 drops) was added to a solution of aldehyde 2 (1.27 mmol, 0.31 g) and resorcinol (1) (1.27 mmol, 0.14 g) in ethyl acetate (1.37 mL) and the reaction mixture was stirred at 100 °C for 1 hour. The reaction was quenched by adding ethyl acetate, then the mixture was cooled at 4 °C for 3 hours and filtered, affording a white solid. The product was insoluble in all organic solvents, thus it was characterized only by HR-ESI-MS and used for the next synthetic step without further purification.

Resorc[4]arene 4. HR-MS: $\text{C}_{64}\text{H}_{59}\text{Br}_4\text{O}_{12}$ $[\text{M}-\text{H}]^-$ Calcd 1335.0740; Found: 1335.0779

Synthesis of Tetrabromo Resorc[4]arene R1. K_2CO_3 (0.7 mmol, 0.1 g) and dimethyl sulfate (0.7 mmol, 66 μL) were added to a solution of crude resorc[4]arene 4 (0.19 g) in acetonitrile (2 mL). The reaction mixture was stirred for 17 hours at 85 °C, then the reaction was quenched with distilled water (50 mL) and extracted with chloroform (3x100 mL). The combined organic layers were dried over anhydrous Na_2SO_4 and the solvent was removed under reduced pressure. The crude product was purified by flash chromatography (CHCl_3 100%→ CHCl_3 /ethyl acetate 98:2) to afford compound R1 (0.07 g, 0.048 mmol) as a white solid in a 15% yield over two steps.

Tetrabromo Resorc[4]arene R1. white solid, mp: 318.5 °C, R_f : 0.79, CHCl_3 /ethyl acetate 95:5. $^1\text{H NMR}$ (400 MHz, CDCl_3) δ 6.58 (d, J = 8.2 Hz, 8 H), 6.48 (d, J = 8.2 Hz, 8 H), 6.45 (s, 2 H), 6.40 (s, 2 H), 6.19 (s, 2 H), 5.77 (s, 2 H), 5.68 (s, 4 H), 4.00 (t, J = 5.8 Hz, 8 H), 3.70 (s, 12 H), 3.67 (s, 12 H), 3.59 (t, J = 6.4 Hz, 8 H), 2.35–2.21 (m, 8 H). $^{13}\text{C NMR}$ (101 MHz, CDCl_3) δ 156.44, 156.19, 155.80, 135.90, 131.78, 130.20, 128.45, 125.50, 124.82, 113.79, 96.75, 95.58, 77.16, 65.54, 56.47, 56.05, 42.14, 32.80, 30.29. HR-MS: $\text{C}_{72}\text{H}_{80}\text{Br}_4\text{NO}_{12}$ $[\text{M} + \text{NH}_4]^+$ Calcd 1466.2414; Found: 1466.2422.

Synthesis of 4-(3-azidopropoxy)benzaldehyde (3). Compound 4 was prepared according to the reported procedure.^[31] The crude was purified by silica gel flash chromatography (petroleum ether 100%→petroleum ether/ethyl acetate 95:5) to afford compound 4 (7.2 mmol, 1.48 g) in 70% yield as a colourless oil. The spectroscopical data were identical to those reported in literature.

4-(3-azidopropoxy)benzaldehyde (3). R_f : 0.55, Petroleum ether/ethyl acetate 7:3. $^1\text{H NMR}$ (400 MHz, CDCl_3) δ 9.89 (s, 1 H), 7.86–7.81 (m, 2 H), 7.03–6.97 (m, 2 H), 4.14 (t, J = 6.0 Hz, 2 H), 3.54 (t, J = 6.5 Hz, 2 H), 2.13–2.05 (m, 2 H).

Synthesis of Resorc[4]arene 5. Concentrated HCl (3 drops) was added to a solution of aldehyde 3 (1.34 mmol, 0.30 g) and resorcinol (1.34 mmol, 0.15 g) in ethyl acetate (1.5 mL), and the reaction mixture was stirred at 100 °C for 2.5 hour. The reaction was quenched by adding ethyl acetate, then the mixture was cooled at 4 °C for 3 hours and filtered, and washed several times with cold ethyl acetate affording resorc[4]arene 5 (0.2 mmol, 0.24 g) in a 60% yield as a red solid.

Resorc[4]arene 5. red solid mp: 236.7 °C, R_f : 0.39, CHCl_3 / CH_3OH 85:15. $^1\text{H NMR}$ (400 MHz, $\text{DMSO}-d_6$) δ 8.48 (s, 4 H), 8.43 (s, 4 H), 6.52 (d, J = 8.7 Hz, 8 H), 6.47 (d, J = 8.7 Hz, 8 H), 6.32 (s, 2 H), 6.30 (s, 2 H), 6.13 (s, 2 H), 5.70 (s, 2 H), 5.47 (s, 4 H), 3.91 (t, J = 6.2 Hz, 8 H), 3.51 (t, J = 6.8 Hz, 8 H), 2.00–1.90 (m, 8 H). $^{13}\text{C NMR}$ (101 MHz, $\text{DMSO}-d_6$) δ 155.55, 152.59, 152.42, 136.58, 131.72, 129.78, 128.79, 121.31, 120.75, 113.09, 101.68, 101.59, 64.39, 47.78, 41.17, 28.31. HR-MS $\text{C}_{64}\text{H}_{59}\text{N}_{12}\text{O}_{12}$ $[\text{M}-\text{H}]^-$ Calcd 1187.4375; Found: 1187.4380.

Synthesis of Tetrazido Resorc[4]arene R2. K_2CO_3 (1.34 mmol, 195 mg) and dimethyl sulfate (1.34 mmol, 127 μL) were added to a solution of resorc[4]arene 5 (0.08 mmol, 0.10 g) in acetonitrile (1 mL). The reaction mixture was stirred for 17 hours at reflux, then the reaction was quenched with distilled water (20 mL) and extracted with chloroform (3x25 mL). The combined organic layers were dried over anhydrous Na_2SO_4 the solvent was removed under vacuum. The crude was purified by crystallization in acetone to afford the compound R2 (0.05 mmol, 70 mg) in a 63% yield as a white solid.

Tetrazido Resorc[4]arene R2. white solid, mp: 265.6 °C, R_f : 0.87, CHCl_3 /EtOAc 95:5. $^1\text{H NMR}$ (400 MHz, CDCl_3) δ

6.59 (d, J = 8.4 Hz, 8 H), 6.48 (d, J = 8.4 Hz, 8 H), 6.45 (s, 2 H), 6.40 (s, 2 H), 6.20 (s, 2 H), 5.79 (s, 2 H), 5.69 (s, 4 H), 3.95 (t, J = 6.0 Hz, 8 H), 3.69 (s, 12 H), 3.66 (s, 12 H), 3.49 (t, J = 6.7 Hz, 8 H), 2.05–1.97 (m, 8 H). $^{13}\text{C NMR}$ (101 MHz, CDCl_3) δ 156.40, 156.17, 155.76, 135.85, 131.73, 130.19, 128.38, 125.46, 124.75, 113.71, 96.67, 95.50, 64.63, 56.43, 56.01, 48.48, 42.12, 29.10. HR-MS $\text{C}_{72}\text{H}_{80}\text{N}_{13}\text{O}_{12}$ $[\text{M} + \text{NH}_4]^+$ Calcd: 1318.6049; Found 1318.6005.

Synthesis of NH_2 -MWCNTs (7): DCC (0.73 mmol, 0.15 g) and NHS (1.3 mmol, 0.15 g) were added to a dispersion of 6 (0.15 g) in THF (30 mL). The mixture was sonicated for 30 minutes, then a mixture of ethylene diamine/THF 2:1 (0.22 mol, 15 mL) (15 mL ethylene diamine, 7.5 mL THF) was added and the dispersion was stirred for 24 hours at room temperature. The nanotubes were filtered through a PTFE membrane (0.2 μm pore size) and washed several times with THF and methanol until reaching pH 7. The nanotubes were dried at 70 °C for 24 hours, affording 0.15 g of 7.

Synthesis of Propargyl-MWCNTs (9): DCC (0.73 mmol, 0.15 g) and NHS (1.3 mmol, 0.15 g) were added to a dispersion of 6 (0.15 g) in DCM (30 mL). The mixture was sonicated for 30 minutes, then propargylamine (3 mL) was added and the dispersion was stirred for 24 hours at room temperature. The nanotubes were filtered through a PTFE membrane (0.2 μm pore size) and washed several times with THF and methanol until reaching pH 7. The nanotubes were dried at 70 °C for 24 hours, affording 0.15 g of 9.

Synthesis of R1-MWCNTs (8): compound R1 (0.014 mmol, 20.2 mg) and Cs_2CO_3 (0.018 mmol, 6 mg) were added to a suspension of 7 (10.6 mg) in dry DMSO (10 mL). The mixture was firstly sonicated for 10 minutes, then it was stirred for 21 hours and sonicated for ten minutes periodically. The suspension was then filtered through a PTFE membrane (0.2 μm pore size) and washed several times with chloroform, water, and methanol. The nanotubes were dried at 70 °C for 24 hours, affording 11 mg of 8.

Synthesis of R2-MWCNTs (10): CuI (0.026 mmol, 5 mg), DIPEA (0.057 mmol, 10 μL) and sodium ascorbate (0.031 mmol, 6 mg) were added to a suspension of 9 (10.7 mg) in degassed acetonitrile (10 mL). The suspension was sonicated and stirred for 10 minutes, then compound R2 (0.008 mmol, 10.1 mg) was added, and the mixture was stirred and sonicated periodically for 41 hours. The suspension was then filtered through a PTFE membrane (0.2 μm pore size) and washed several times with an aqueous solution of EDTA 13.4 mM, and then with chloroform,

water, and methanol. The nanotubes were dried at 70 °C for 24 hours, affording 11 mg of 10.

Synthesis of R2-p-MWCNTs (12): compound **R2** (0.015 mmol, 19.5 mg) was added to a suspension of **11** (5.5 mg) in degassed o-DCB (6 mL). The suspension was stirred and periodically sonicated at 160 °C for 4 days. The suspension was then filtered through a PTFE membrane (0.2 μm pore size) and washed several times with chloroform. The nanotubes were dried at 70 °C for 24 hours, affording 6 mg of **12**.

XPS measurements. XPS data were obtained with a modified Omicron NanoTechnology MXPS system by exposing the samples to achromatic Mg Kα photons ($h\nu = 1253.6$ eV), generated operating the anode at 14 kV, 13 mA. Experimental spectra were theoretically reconstructed by symmetric pseudo-Voigt functions (linear combinations of Gaussian and Lorentzian peaks), and a Shirley or a linear background. XPS atomic ratios ($\pm 10\%$ associated error) were obtained from experimentally determined area ratios, corrected for the corresponding calculated atomic cross-sections^[69] and for a square root dependence of the photoelectrons kinetic energies. All samples underwent charging under X-rays because of their mounting on insulating Teflon tape, covering the tips. This procedure was applied to exclude from the useful C 1s and O 1s energy range, the presence of carbon and oxygen contribution coming from the underlying tips. Quantitation with C 1s peak was conducted after numerical removal, using a software routine, of the contribution of Mg Kα₃ and Mg Kα₄ components. The binding energy scale for pure **R1** and **R2**, for the anchored compounds and for MWCNTs and **7** was referenced to the lowest-lying C 1s component due to the carbon atoms of the aromatic rings.

Electrode modification. Glassy Carbon Electrode Modification. A bare glassy carbon (GC) electrode was polished on a micro cloth for three minutes with 0.03 μm and 0.05 μm alumina suspensions. After each polishing step, the electrodes were sonicated for 3 minutes in milliQ water and ethanol. The electrodes' surfaces were thus rinsed with ethanol and let dry. The cleaned GC electrodes were modified by drop cast with 4 μL of a 1 mg mL⁻¹ **8** dispersion in a 30:70 EtOH/H₂O mixture and sonicated for 30 minutes. Ab-SPS1 and SPS1 were stored at -20 °C in aliquots of 10–1 mg/L and 10–500 ng/mL in 20 mM PBS buffer pH 7.4, respectively to avoid repeated freeze and thaw cycles. All solutions were prepared using Milli-Q water (18.2 MΩ/cm, Millipore, Bedford, MA, USA). Then, 5 μL of the antibody solutions (0.1–1 μg mL⁻¹) were dropped on the modified GC/R1-MWCNTs surface and incubated for 30 min. The surface was gently rinsed with the incubation buffer. The antibody solutions were diluted in MES buffer at pH 5.4 and 6, in HEPES buffer at pH 6.5 and in PBS at pH 7.4 and 8.0. SPS1 standards in PBS of 0.1–100 ng mL⁻¹ and gently rinsed in the incubation buffer. After the surface got dry, 0.1 mg/mL of BSA were incubated for 20 minutes. The SPS1 calibration was performed by incubating (0.1–100 ng/mL) SPS1 protein for 30 minutes.

Electrochemical characterization. The potentiostat was connected to a classical three-electrode electrochemical cell with a SCE reference electrode (RE) a graphite counter electrode (CE) and GC as a working electrode (WE). The measurements were performed in a 1.1 mM [Fe(CN)₆]^{3-/4-}, 100 mM KCl between a potential between [-0.3 ; 0.7] V vs SCE. The DPV measurements were performed using a 1.1 mM [Fe(CN)₆]^{3-/4-}, 100 mM KCl in PBS buffer 10 mM pH 7.4. The electrode characterization was performed by CV measurements at different scan rates (5 mV/s ÷ 200 mV/s) in a 1.1 mM solution of [Fe(CN)₆]^{3-/4-} and 100 mM KCl. The electrode active area (A_{EL}) was obtained by using the Randles-Ševčík equation (eq. 1),^[70] where I_p (measured in amperes) is the

peak current, n is the number of electrons transferred in the redox reaction, A (cm²) is the electroactive surface area, D (cm² × s⁻¹) is the diffusion of the redox probe (7.6×10^{-6} cm² × s⁻¹ for [Fe(CN)₆]^{3-/4-}), C (mol × cm⁻³) is the concentration of the redox probe, and v (V × s⁻¹) is the scan rate.^[51]

$$I_p = 2.69 \times 10^5 n^{3/2} A C_0 D^{1/2} v^{1/2} \quad (1)$$

Random immobilization platform (GC/ox-MWCNTs/AbSPS1)

The random platform was developed as follows. 1 mg of ox-MWCNTs were sonicated in 1 mL of a mixture 30:70 EtOH/H₂O until it turned homogeneous. Next, 4 μL were drop casted on a clean GC electrode and allowed to dry. The excess was removed by gently rinsing with water, and once the surface was dry, the electrode was treated with a mixture of a freshly prepared 0.5 mM/0.1 mM of EDC/NHS solution in MES buffer pH 5.4. The mild acidic environment promotes the activation of the carboxylic groups exposed on the ox-MWCNTs surface for the amine coupling with AbSPS1 amino groups. After 15 minutes, the surface was gently rinsed with MES buffer, and then, 4 μL of 0.2 μg/mL AbSPS1 solution in PBS buffer was incubated on the surface for 30 minutes. The surface was deactivated by ethanolamine treatment for 20 minutes and the sensing surface was then incubated with different SPS1 standard solutions in PBS.

Supporting Information

NMR spectra; morphological characterization; XPS characterization; electrochemical characterization; computational methods.

Funding Sources

The work was financially supported by the Excellence Departments grant from MIUR (Art. 1, commi 314-337 Legge 232/2016) to the Department of Chemistry and Technology of Drugs and Sapienza University of Rome under Grants "Progetti Ateneo 2020" and "Progetti Ateneo 2021".

Acknowledgements

The authors want to thank Prof. Giancarlo Fabrizi for providing 1-butyl-3-methylimidazolium tetrafluoroborate, and Prof. Aldo Lagana and Prof. Anna Laura Capriotti for performing high-resolution mass spectrometry analyses. Open Access funding provided by Università degli Studi di Roma La Sapienza within the CRUI-CARE Agreement.

Conflict of Interest

The authors declare no conflict of interest.

Data Availability Statement

The data that support the findings of this study are available in the supplementary material of this article.

Keywords: biosensor · carbon nanotubes · resorc[4]arenes · SARS-CoV-2 · site-directed immobilization

- [1] Y. Zhou, Y. Fang, R. P. Ramasamy, *Sensors* **2019**, *19*, 392.
- [2] T. Han, A. Nag, S. Chandra Mukhopadhyay, Y. Xu, *Sens. Actuators A* **2019**, *291*, 107–143.
- [3] A. L. Khalaf, T. S. Hasan, H. A. Abdulbari, W. A. Kadhim, M. H. Yaacob, *J. Mater. Res. Technol.* **2021**, *12*, 1738–1746.
- [4] M. N. Norizan, M. H. Moklis, S. Z. Ngah Demon, N. A. Halim, A. Samsuri, I. S. Mohamad, V. F. Knight, N. Abdullah, *RSC Adv.* **2020**, *10*, 43704–43732.
- [5] D. C. Ferrier, K. C. Honeychurch, *Biosensors* **2021**, *11*, 486.
- [6] R. A. Potyralo, C. Surman, N. Nagraj, A. Burns, *Chem. Rev.* **2011**, *111*, 7315–7354.
- [7] M. Holzinger, J. Abraham, P. Whelan, R. Graupner, L. Ley, F. Hennrich, M. Kappes, A. Hirsch, *J. Am. Chem. Soc.* **2003**, *125*, 8566–8580.
- [8] J. Liu, Z. Cao, Y. Lu, *Chem. Rev.* **2009**, *109*, 1948–1998.
- [9] R. Dubey, D. Dutta, A. Sarkar, P. Chattopadhyay, *Nanoscale Adv.* **2021**, *3*, 5722–5744.
- [10] A. M. Díez-Pascual, *Macromolecules* **2021**, *1*, 64–83.
- [11] N. G. Sahoo, S. Rana, J. W. Cho, L. Li, S. H. Chan, *Prog. Polym. Sci.* **2010**, *35*, 837–867.
- [12] N. Karousis, N. Tagmatarchis, D. Tasis, *Chem. Rev.* **2010**, *110*, 5366–5397.
- [13] S. Mohajeri, A. Dolati, S. S. Rezaie, *J. Chem. Sci.* **2019**, *131*, 1–18.
- [14] F. Polli, C. D'Agostino, R. Zumpano, V. de Martino, G. Favero, L. Colangelo, S. Minisola, F. Mazzei, *Talanta* **2023**, *251*, 123755.
- [15] E. Katz, I. Willner, *ChemPhysChem* **2004**, *5*, 1084–1104.
- [16] N. Maheshwari, M. Tekade, N. Soni, P. Ghode, M. C. Sharma, P. K. Deb, R. K. Tekade, in *Advances in Pharmaceutical Product Development and Research* (Ed.: R. K. Tekade), Academic Press, **2019**, pp. 613–637.
- [17] D. Cui, *J. Nanosci. Nanotechnol.* **2007**, *7*, 1298–1314.
- [18] R. Pinalli, A. Pedrini, E. Dalcanale, *Chem. Soc. Rev.* **2018**, *47*, 7006–7026.
- [19] D. Quaglio, F. Polli, C. del Plato, G. Cianfoni, C. Tortora, F. Mazzei, B. Botta, A. Calcaterra, F. Ghirga, *Supramol. Chem.* **2021**, *26*, 8400.
- [20] Y.-Y. Zhao, J.-M. Yang, X.-Y. Jin, H. Cong, Q. Ge, M. Liu, Z. Tao, *Curr. Org. Chem.* **2020**, *24*, 265–290.
- [21] I. D'Acquarica, A. Calcaterra, F. Sacco, F. Balzano, F. Aiello, A. Tafi, N. Pesci, G. Uccello-Barretta, B. Botta, *Chirality* **2013**, *25*, 840–851.
- [22] D. Quaglio, G. Zappia, E. de Paolis, S. Balducci, B. Botta, F. Ghirga, *Org. Chem. Front.* **2018**, *5*, 3022–3055.
- [23] B. Botta, M. Cassani, I. D'Acquarica, D. Misiti, D. Subissati, D. G. Monache, *Curr. Org. Chem.* **2005**, *9*, 337–355.
- [24] F. Buonsenso, F. Ghirga, I. Romeo, G. Siani, S. Pilato, D. Quaglio, M. Pierini, B. Botta, A. Calcaterra, *Int. J. Mol. Sci.* **2021**, *22*, 11785.
- [25] G. Bocchinfuso, C. Mazzuca, C. Saracini, M. Venanzi, L. Micheli, G. Palleschi, A. Palleschi, *Microchim. Acta* **2008**, *163*, 195–202.
- [26] G. A. Evtugyn, E. E. Stoikova, R. v Shamagsumova, *Russ. Chem. Rev.* **2011**, *79*, 1071–1097.
- [27] P. B. Crowley, *Acc. Chem. Res.* **2022**, *55*, 2019–2032.
- [28] D. Quaglio, L. Mangiardi, G. Venditti, C. del Plato, F. Polli, F. Ghirga, G. Favero, M. Pierini, B. Botta, F. Mazzei, *Chem. Eur. J.* **2020**, *26*, 8400–8406.
- [29] M. Drozd, S. Karoń, E. Malinowska, *Sensors* **2021**, *21*, 3781.
- [30] L.-F. Pan, X.-B. Wang, S.-S. Xie, S.-Y. Li, L.-Y. Kong, *MedChemComm* **2014**, *5*, 609–616.
- [31] M. D. Yilmaz, O. A. Bozdemir, E. U. Akkaya, *Org. Lett.* **2006**, *8*, 2871–2873.
- [32] L. Ngodwana, D. J. Kleinhans, A.-J. Smuts, W. A. L. van Otterlo, G. E. Arnott, *RSC Adv.* **2013**, *3*, 3873–3876.
- [33] R. S. Patil, C. Zhang, J. L. Atwood, *Chem. Eur. J.* **2016**, *22*, 15202–15207.
- [34] Y. Wang, Z. Iqbal, S. v Malhotra, *Chem. Phys. Lett.* **2005**, *402*, 96–101.
- [35] > *Surface Modification of Nanotube Fillers* (Ed.: V. Mittal), Wiley-VCH, **2011**.
- [36] R. N. Salvatore, A. S. Nagle, S. E. Schmidt, K. W. Jung, *Org. Lett.* **1999**, *1*, 1893–1896.
- [37] J. F. Watts, *Surf. Interface Anal.* **1993**, *20*, 267.
- [38] J. Han, C. Gao, *Nano-Micro Lett.* **2010**, *2*, 213–226.
- [39] I. Kumar, S. Rana, C. V. Rode, *J. Nanosci. Nanotechnol.* **2008**, *8*, 3351.
- [40] Z. Guo, L. Liang, J. Liang, Y. Ma, X. Yang, D.-M. Ren, Y. Chen, J.-Y. Zheng, *J. Nanopart. Res.* **2008**, *10*, 1077–1083.
- [41] P. Fortgang, T. Tite, V. Barnier, N. Zehani, C. Maddi, F. Lagarde, A.-S. Loir, N. Jaffrezic-Renault, C. Donnet, F. Garrelie, C. Chaix, *ACS Appl. Mater. Interfaces* **2016**, *8*, 1424–1433.
- [42] S. Ciampi, T. Böcking, K. A. Kilian, M. James, J. B. Harper, J. J. Gooding, *Langmuir* **2007**, *23*, 9320–9329.
- [43] J. P. Collman, N. K. Devaraj, T. P. A. Eberspacher, C. E. D. Chidsey, *Langmuir* **2006**, *22*, 2457–2464.
- [44] Y. Li, J. Wang, C. Cai, *Langmuir* **2011**, *27*, 2437–2445.
- [45] M. Dionisio, J. M. Schnorr, V. K. Michaelis, R. G. Griffin, T. M. Swager, E. Dalcanale, *J. Am. Chem. Soc.* **2012**, *134*, 6540–6543.
- [46] G. Tuci, C. Zafferoni, P. D'Ambrosio, S. Caporali, M. Ceppatelli, A. Rossin, T. Tsoufis, M. Innocenti, G. Giambastiani, *ACS Catal.* **2013**, *3*, 2108–2111.
- [47] M. M. Mahat, M. Mawad, G. W. Nelson, S. Fearn, R. G. Palgrave, D. J. Payne, M. M. Stevens, *J. Mater. Chem. C* **2015**, *3*, 7180–7186.
- [48] G. Wang, R. Liang, L. Liu, B. Zhong, *Electrochim. Acta* **2014**, *115*, 183–188.
- [49] R. Zumpano, F. Polli, C. D. Agostino, R. Antiochia, G. Favero, *Electrochemistry* **2020**, 1–24.
- [50] T. F. Otero, J. G. Martinez, K. Asaka, *Front. Mater.* **2016**, *3*, DOI 10.3389/fmats.2016.00003.
- [51] G. Fusco, P. Bollella, F. Mazzei, G. Favero, R. Antiochia, C. Tortolini, *J. Anal. Methods Chem.* **2016**, *2016*, 47–55.
- [52] V. S. Ijeri, J. R. Nair, S. Zonarini, C. Gerbaldi, *Global J. Anal. Chem.* **2011**, *2*.
- [53] V. Ijeri, F. Vocanson, C. Martelet, N. Jaffrezic-Renault, *Electroanalysis* **2007**, *19*, 510–514.
- [54] H. Chen, F. Liu, F. Qi, K. Koh, K. Wang, *Int. J. Mol. Sci.* **2014**, *15*, 5496–5507.
- [55] Y. Lee, E. K. Lee, Y. W. Cho, T. Matsui, I. C. Kang, T. S. Kim, M. H. Han, *Proteomics* **2003**, *3*, 2289–2304.
- [56] A. S. Mahadevi, G. N. Sastry, *Chem. Rev.* **2013**, *113*, 2100–2138.
- [57] R. Pinalli, G. Brancatelli, A. Pedrini, D. Menozzi, D. Hernández, P. Ballester, S. Geremia, E. Dalcanale, *J. Am. Chem. Soc.* **2016**, *138*, 8569–8580.
- [58] K. O. Ramberg, S. Engilberge, T. Skorek, P. B. Crowley, *J. Am. Chem. Soc.* **2021**, *143*, 1896–1907.
- [59] S. Yamada, *Coord. Chem. Rev.* **2020**, *415*, 213301.
- [60] K. Kumar, S. M. Woo, T. Siu, W. A. Cortopassi, F. Duarte, R. S. Paton, *Chem. Sci.* **2018**, *9*, 2655–2665.
- [61] J. Buijs, J. W. T. Lichtenbelt, W. Norde, J. Lyklema, *Colloids Surf. B* **1995**, *5*, 11–23.
- [62] F. Krebs, C. Scheller, K. Grove-Heike, L. Pohl, H. Wätzig, *Electrophoresis* **2021**, *42*, 687–692.
- [63] M. R. Pergande, S. M. Cologna, *Proteomes* **2017**, *5*, 4.
- [64] B. Sonmez, S. Sayin, E. E. Yalcinkaya, D. A. Selec, H. B. Yildiz, D. O. Demirkol, S. Timur, *RSC Adv.* **2014**, *4*, 62895–62902.
- [65] X. Xia, *Viruses* **2021**, *13*, 1–16.
- [66] L. Fabiani, M. Saroglia, G. Galatà, R. de Santis, S. Fillo, V. Luca, G. Faggioni, N. D'Amore, E. Regalbutto, P. Salvatori, G. Terova, D. Moscone, F. Lista, F. Arduini, *Biosens. Bioelectron.* **2021**, *171*, 112686.
- [67] H. Haji-Hashemi, M. R. Safarnejad, P. Norouzi, M. Ebrahimi, M. Shahmirzaie, M. R. Ganjali, *Anal. Biochem.* **2019**, *566*, 102–106.
- [68] D. Y. Ong, S. Chiba, *Synthesis* **2020**, *52*, 1369–1378.
- [69] J. H. Scofield, *J. Electron Spectrosc. Relat. Phenom.* **1976**, *8*, 129–137.
- [70] G. Favero, G. Fusco, F. Mazzei, F. Tasca, R. Antiochia, *Nanomaterials* **2015**, *5*, 1995–2006.

Manuscript received: January 13, 2023
 Revised manuscript received: March 2, 2023
 Accepted manuscript online: March 3, 2023
 Version of record online: April 4, 2023